STRUCTURAL CONTROL AND HEALTH MONITORING
Struct. Control Health Monit. 2017; 24: e1889
Published online 29 May 2016 in Wiley Online Library (wileyonlinelibrary.com). DOI: 10.1002/stc.1889

Identification of time-varying cable tension forces based on adaptive sparse time-frequency analysis of cable vibrations

Yuequan Bao[1,2,3,*,†], Zuoqiang Shi[4], James L. Beck[1], Hui Li[2,3] and Thomas Y. Hou[1]

[1]*Computing and Mathematical Sciences, California Institute of Technology, Pasadena, CA 91125, USA*
[2]*Key Lab of Structures Dynamic Behavior and Control of the Ministry of Education, Harbin Institute of Technology, Harbin 150090, China*
[3]*School of Civil Engineering, Harbin Institute of Technology, Harbin 150090, China*
[4]*Mathematical Sciences Center, Tsinghua University, Beijing 100084, China*

SUMMARY

For cable bridges, the cable tension force plays a crucial role in their construction, assessment and long-term structural health monitoring. Cable tension forces vary in real time with the change of the moving vehicle loads and environmental effects, and this continual variation in tension force may cause fatigue damage of a cable. Traditional vibration-based cable tension force estimation methods can only obtain the time-averaged cable tension force and not the instantaneous force. This paper proposes a new approach to identify the time-varying cable tension forces of bridges based on an adaptive sparse time-frequency analysis method. This is a recently developed method to estimate the instantaneous frequency by looking for the sparsest time-frequency representation of the signal within the largest possible time-frequency dictionary (i.e. set of expansion functions). In the proposed approach, first, the time-varying modal frequencies are identified from acceleration measurements on the cable, then, the time-varying cable tension is obtained from the relation between this force and the identified frequencies. By considering the integer ratios of the different modal frequencies to the fundamental frequency of the cable, the proposed algorithm is further improved to increase its robustness to measurement noise. A cable experiment is implemented to illustrate the validity of the proposed method. For comparison, the Hilbert–Huang transform is also employed to identify the time-varying frequencies, which are then used to calculate the time-varying cable-tension force. The results show that the adaptive sparse time-frequency analysis method produces more accurate estimates of the time-varying cable tension forces than the Hilbert–Huang transform method. Copyright © 2016 John Wiley & Sons, Ltd.

Received 26 May 2015; Revised 20 March 2016; Accepted 1 May 2016

KEY WORDS: structural health monitoring; time-varying cable tension identification; adaptive sparse time-frequency analysis; time-frequency dictionary; Hilbert–Huang transform

1. INTRODUCTION

Structural health monitoring systems for the safety of structures have been widely investigated and installed on many civil infrastructure systems, such as long-span bridges, offshore structures, large dams, nuclear power stations, tall buildings and other large spatial structures [1–4]. For large span bridges, such as cable-stayed and suspension bridges, the cables are a crucial element for overall safety of the structure. The cable tension forces vary in real time because of the loads from moving vehicles and other environmental effects, and this variation in cable tension forces may cause fatigue damage. Therefore, estimation of the time-varying cable tension forces from cable vibration measurements or special force sensors on the cables is important for the maintenance and safety assessment of cable-based bridges.

*Correspondence to: Yuequan Bao, School of Civil Engineering, Harbin Institute of Technology, Harbin, China.
†E-mail: baoyuequan@hit.edu.cn

Vibration-based methods for estimating cable tension forces use a relation between the natural frequency of the cable vibrations and the tension force in the cable. These nondestructive monitoring methods are widely studied and often are used in practice with the advantages of being inexpensive and convenient to install. The existing vibration-based estimation methods can be classified into four categories depending on what cable vibration theory they use [5].

The first category of estimation methods utilizes the flat taut string theory that neglects both sag-extensibility and bending stiffness

$$F = 4mL^2 f_1^2 \tag{1}$$

where F is the cable tension forces; f_1 is the fundamental natural frequency; and m and L are the mass density and length of cable, respectively. Casas [6] used Eqn (1) to measure cable tension forces in the Alamillo Bridge with accelerometers installed on cables. Gentile [7] used microwave remote sensing to measure the vibration response in the longer cables of two cable-stayed bridges and then predicted the cable tensions from natural frequencies using the formula as Eqn (1). Kim and Shin [8] have made a comparative study of several tension estimation methods for cable supported bridges and they concluded that taut string theory is a good tool for a first approximation because of its simplicity and quick calculation. Ren *et al.* [9] discussed the effects of sag and the bending moment on the fundamental frequencies of cables under ambient excitation and concluded that these frequencies are close to the fundamental frequency of a taut-string even when the cable sag and bending stiffness effects are taken into account. Then they used these frequency differences to replace the fundamental frequency in the taut string theory formula and estimated the cable tension forces in laboratory tests and in a field test for the stay cables from the Qingzhou Bridge in China.

For the second category of estimation methods, sag-extensibility is considered but bending stiffness is ignored. Based on this theory, Russell and Lardner [10] experimentally investigated estimation of cable tension forces. On their approach, additional information consisting of the unstrained length of the cable is needed and a nonlinear characteristic equation is solved by trial and error [10]. However, the unstrained length is often not available in practice [5].

For the third category of estimation methods, an axially loaded beam considering bending stiffness but not sag-extensibility is used [11]

$$F = 4mL^2\left(\frac{f_n}{n}\right)^2 - \frac{EI}{L^2}(n\pi)^2 \tag{2}$$

where f_n is the nth modal frequency, and EI denotes the flexural rigidity of cable. However, Eqn (2) may cause errors for short and stout cables because this formula is derived from an axially tensioned beam with hinged end boundaries rather than a fixed one [12]. Fang and Wang [12] proposed a curve-fitting technique to solve the free vibration equation of the cable with two fixed ends, which gave an explicit formula for cable tension estimation, and they then verified their formula with available experimental results and finite element solutions. Sim *et al.* [13] developed a wireless cable tension monitoring system using MEMSIC's Imote2 (Intel Corporation, Santa Clara, CA, USA) smart sensors, in which Eqn (2) is implemented on the sensors.

The last category of estimation methods takes account of both sag-extensibility and bending stiffness using a practical formula. Zui *et al.* [14] developed a set of such formulas that were deduced from the cable's free vibration with some assumptions for simplicity. Kim and Park [5] proposed an approach to estimate cable tension force from measured natural frequencies, while simultaneously identifying flexural and axial rigidities of a cable system. They use a finite element model that considers both sag-extensibility and flexural rigidities and then a frequency-based sensitivity-updating algorithm is applied to identify the model. Liao *et al.* [15] developed a model-based method to simultaneously identify cable tension and other structural parameters from the identified modal frequencies by using a finite element model of the cables combined with a least-squares optimization scheme. Cho *et al.* [16] embedded the cable tension force estimation equations proposed by Zui *et al.* [14] into wireless sensors to produce an automated cable tension force monitoring system for cable-stayed bridges.

All of these vibration-based methods are usually not able to estimate the time-varying cable tension forces, but only their average values. In contrast, Li *et al.* [17] proposed an extended Kalman filter

DOI: 10.1002/stc

based method to estimate the time-varying cable tension force using the measured acceleration data, but it also needs wind speed data from the bridge. Yang *et al.* [18] proposed a method to identify time-varying cable tension forces from acceleration data via an unsupervised learning algorithm called complexity pursuit. The method is based on flat taut string theory and tracks the time-varying cable frequency using data from two accelerometers on a cable.

In addition to the vibration-based methods for bridge cable tension force identification, direct measurements using traditional force sensors and elasto-magnetic (EM) sensors have also been used. The traditional force sensor is used in a series connection with the cable to measure the strain, either by a vibrating wire transducer, strain gauge, hydraulic pressure sensor or Fiber Bragg Grating sensor. The series connection means that these sensors are not readily replaceable, and they are difficult to calibrate under the high stress states occurring in field applications. In addition, they tend to have unstable long-term performance. These sensors are therefore not widely used for long-term monitoring of bridge cables. On the other hand, EM sensors have been used to measure static cable tensions based on the variation under stress of the magnetic permeability of a ferromagnetic material [19]. Field tests and applications of EM sensors for monitoring the cable tension in some bridges have been reported [20,21].

For the identification of time-varying cable tension forces, one idea is to estimate these forces by identifying the time-varying natural frequencies of the cable through time-frequency analysis of the cable vibration signal. For the frequency varying through time over a small range and with noisy data, a high resolution time-frequency analysis method is needed that is insensitive to noise. Recently, a new adaptive signal analysis method has been developed to study trends and instantaneous frequencies for nonlinear and non-stationary time series data [22–24]. By combining the Empirical Mode Decomposition method [25] and Compressive Sensing theory [26–28], this method is able to look for the sparsest time-frequency representation of the signal within a dictionary consisting of Empirical Mode Decomposition intrinsic mode functions. The advantages of this novel adaptive sparse time-frequency analysis method are its high resolution in the time-frequency domain and its robustness to measurement noise. Here, we employ this method to estimate the time-varying cable tension force by using only measurements of the cable vibrations obtained from accelerometers.

2. ADAPTIVE SPARSE TIME-FREQUENCY ANALYSIS

Typically, the time-frequency analysis method consists of two parts: a large dictionary of time-frequency functions used to represent the signal and a decomposition method to decompose the signal over the dictionary.

As an example of a dictionary, the Fourier transform, one of the most widely used frequency analysis methods, uses the well-known Fourier harmonic basis functions

$$\{\sin 2\pi kt,\ \cos 2\pi kt :\ k = 0, 1, 2, \cdots\} \tag{3}$$

where we assume that time has been scaled for the signal so that $t \in [0, 1]$. For any signal $f(t)$, $t \in [0, 1]$, we have the following Fourier expansion:

$$f(t) = a_0 + \sum_{k=1}^{M} (a_k \cos 2k\pi t + b_k \sin 2k\pi t) \tag{4}$$

where the coefficients a_k, b_k can be obtained by the Fourier integral, and the frequency for each component is $2k\pi$, which is the derivative of the phase function $2k\pi t$.

The Fourier series is a powerful tool which has been widely used in many different applications. However, in many applications of time-frequency analysis, the Fourier series is not adequate because the signal frequencies are time varying, whereas the frequencies given by the Fourier basis functions in Eqn (3) are all constants over the whole time span. For example, consider a simple chirp signal $f(t) = \cos 50\pi t^2$, $t \in [0, 1]$. Intuitively, the frequency should continuously increase as time grows, but this information is not revealed by its Fourier coefficients as can be seen in Figure 1.

In order to get a time-varying frequency, one natural idea is to enlarge the dictionary of the time-frequency functions to incorporate functions with time-changing frequency. One such generalization is to replace the Fourier basis by the so-called AM–FM signals, which can be written $a(t)\cos\theta(t)$,

DOI: 10.1002/stc

where we require that $a(t)$ and the derivative of $\theta(t)$, $\dot{\theta}(t)$, are less oscillatory than $\cos\theta(t)$. 'Less oscillatory' means that over a few oscillations of $\cos\theta(t)$, the variation of $a(t)$ and $\dot{\theta}(t)$ is small so that that they can be well approximated by constants during these few oscillations. Then in this short time interval, the signal is decomposed approximately over the Fourier basis, which means that the frequency $\omega(t)$ can be defined to be the derivative of the phase function

$$\omega(t) = \dot{\theta}(t) \tag{5}$$

We can therefore define informally the dictionary of AM–FM signals by

$$D = \left\{a(t)\cos\theta(t) :\ a(t),\ \dot{\theta}(t) \text{ are less oscillatory than } \cos\theta(t)\right\} \tag{6}$$

To give a rigorous definition of 'less oscillatory', we define a linear space $V(\theta)$,

$$V(\theta) = span\left\{1,\ \left(\cos\left(\frac{k\theta(t)}{L_\theta}\right)\right)_{1\le k\le \lambda L_\theta},\ \left(\sin\left(\frac{k\theta(t)}{L_\theta}\right)\right)_{1\le k\le \lambda L_\theta} : k = 1,\ldots,\lambda L_\theta\right\} \tag{7}$$

where $\lambda \le 1/2$ is a parameter to control the smoothness and $L_\theta = (\theta(1) - \theta(0))/2\pi$ is the number of oscillations. A function, $a(t)$, is said to be 'less oscillatory' than $\cos\theta(t)$ if and only if $a(t) \in V(\theta)$. Then, the dictionary D can be made well defined by

$$D = \left\{a(t)\cos\theta(t) : a(t), \dot{\theta}(t) \in V(\theta)\right\} \tag{8}$$

Notice that $V(\theta)$ is different for each choice of $\theta(t)$, and D includes all possible choice of $\theta(t)$. So, the dictionary D is a huge dictionary that includes most of the published time-frequency dictionaries, such as the Fourier dictionary in Eqn (3), the Gabor dictionary and the wavelet dictionary.

For an arbitrary signal $f(t)$, we need to decompose it over the above dictionary D to within a given tolerance threshold ε:

$$f(t) = \sum_{k=1}^{M} a_k(t)\cos\theta_k(t) + r(t) \tag{9}$$

where $r(t)$ is a small residual satisfying $\|r\|_2 \le \varepsilon$. For each component, its frequency is defined as

$$\omega_k(t) = \dot{\theta}_k(t) \tag{10}$$

The remaining problem is how to choose the decomposition. In Fourier analysis, because the basis is orthogonal, the unique decomposition is obtained by the Fourier transform. Unfortunately, the dictionary D in Eqn (8) is highly redundant (the functions are not linearly independent) which means that the decomposition is not unique. Taking the chirp signal in Figure 1 as an example; obviously both $f(t)\cos(50\pi t^2)$ and its Fourier series are feasible decompositions using dictionary D, but the decomposition $\cos(50\pi t^2)$ is the one we want because this decomposition gives us an instantaneous frequency. A fundamental feature of this decomposition is that it is very sparse. The whole signal is represented by only one component while there are about 100 components in the Fourier series (Figure 1).

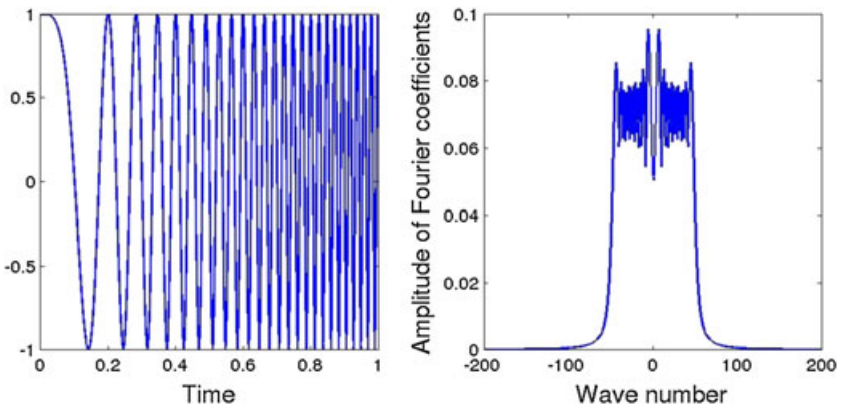

Figure 1. The chirp signal (left) and its Fourier coefficients (right).

DOI: 10.1002/stc

For general time-frequency analysis of signals, we therefore look for the sparsest decomposition among all feasible decompositions based on dictionary D in Eqn (8), which is defined informally by the following optimization problem:

$$\begin{aligned} &\underset{(a_k)_{1\le k\le M},\,(\theta_k)_{1\le k\le M}}{\text{Minimize}} \quad M \\ &\text{Subject to}: \quad \left\| f(t) - \sum_{k=1}^{M} a_k(t)\cos\,\theta_k(t) \right\|_2 \le \varepsilon, \text{ on } [0,1] \\ &\qquad\qquad a_k(t)\,\cos\,\theta_k(t) \in D \end{aligned} \tag{11}$$

If the signal $f(t)$ is completely known on [0, 1], the optimization problem in Eqn (11) can be approximately solved by the following nonlinear matching pursuit method [23]:

Step 1 Let

$$r_0(t) = f,\ k = 1 \tag{12}$$

Step 2 Solve the following nonlinear least-squares problem for functions a_k and θ_k on [0, 1]

$$(a_k(t), \theta_k(t)) \in \underset{a(t),\,\theta(t)}{\text{Argmin}} \|r_{k-1}(t) - a(t)\cos\theta(t)\|_2^2, \ \text{ subject to}: \ a(t)\,\cos\,\theta(t) \in D \tag{13}$$

Step 3 Update the residual

$$r_k(t) = f(t) - \sum_{i=1}^{k} a_i(t)\cos\theta_i(t) \tag{14}$$

Step 4 If $\|r_k(t)\|_2 < \varepsilon$, stop, where ε is a chosen residual threshold. Otherwise, set $k = k+1$ and go to Step 2.

In the above algorithm, the key part is to solve the nonlinear least-squares problem in Step 2. It is found that this problem can be approximately solved by using Gauss–Newton type iteration along with the Fast Fourier transform. By combining these techniques, an efficient method was proposed in [22]. Under some assumptions, the convergence of this method has been proved [24].

In real applications, all the signals are given at discrete time points. Suppose that the discrete signal vector $\mathbf{f} \in \mathfrak{R}^N$ is the measurements of $f(t)$ over discrete time points $t_j = j\Delta t$, $\Delta t = 1/N$, $j = 1, \ldots, N$. The discrete phase function $\boldsymbol{\theta}_k \in \mathfrak{R}^N$ is the sample of $\theta_k(t)$ over discrete time points t_j. Then the discrete form of Eqn (13) for $k = 1$ is given by

$$\min_{\mathbf{x},\boldsymbol{\theta}} \|\mathbf{f} - \boldsymbol{\Phi}_\theta \cdot \mathbf{x}\|_2, \ \text{ subject to}: \ \dot{\boldsymbol{\theta}} \in V(\boldsymbol{\theta}) \tag{15}$$

where $V(\boldsymbol{\theta})$ is discrete space version of $V(\theta)$ in Eqn (7); $\boldsymbol{\Phi}_\theta$ is a $N \times (2\lambda L_\theta + 1)$ matrix with the jth row given by:

$$\boldsymbol{\Phi}_{\theta j} = \left(\cos\theta\left(t_j\right)\right)\boldsymbol{\Pi}_{\theta j},\ j = 1, \ldots, N \tag{16}$$

and $\boldsymbol{\Pi}_{\theta j}$ is the jth row of matrix $\boldsymbol{\Pi}_\theta$ defined by:

$$\boldsymbol{\Pi}_{\theta j} = \left[1, \left(\cos\left(\frac{k\theta\left(t_j\right)}{L_\theta}\right)\right)_{1\le k\le \lambda L_\theta}, \left(\sin\left(\frac{k\theta\left(t_j\right)}{L_\theta}\right)\right)_{1\le k\lambda L_\theta}\right],\ j = 1, \ldots, N \tag{17}$$

In Eqn (15), $\mathbf{x}$ is the vector of coefficients of the envelope $a(t)$ in $V(\theta)$; if $\mathbf{a} \in \mathfrak{R}^N$ is the discrete vector of $a(t)$ over discrete time points $t_j = j\Delta t$, $\Delta t = 1/N$, $j = 1, \ldots, N$, then $\mathbf{a} = \boldsymbol{\Pi}_\theta \cdot \mathbf{x}$. The constraint $\dot{\boldsymbol{\theta}} \in V(\boldsymbol{\theta})$ is enforced by setting $\dot{\boldsymbol{\theta}} = \boldsymbol{\Pi}_\theta \cdot \mathbf{z}$, where $\mathbf{z}$ is the coefficient vector. Then the discrete version of the matching pursuit algorithm is

Step 1 Let

$$\mathbf{r}_0 = \mathbf{f},\ k = 1 \tag{18}$$

Step 2 Solve the following nonlinear least-squares problem for vectors $\mathbf{x}_k$ and $\boldsymbol{\theta}_k$ on [0, 1]

$$(\mathbf{x}_k, \boldsymbol{\theta}_k) \in \underset{\mathbf{x},\,\boldsymbol{\theta}}{\text{Argmin}} \|\mathbf{r}_{k-1} - \boldsymbol{\Phi}_\theta \cdot \mathbf{x}\|_2^2, \text{subject to}: \ \dot{\boldsymbol{\theta}} \in V(\boldsymbol{\theta}) \tag{19}$$

and set $\mathbf{a}_k = \boldsymbol{\Pi}_\theta \cdot \mathbf{x}_k$.

DOI: 10.1002/stc

Step 3 Update the residual

$$\mathbf{r}_k = \mathbf{f} - \sum_{i=1}^{k} \mathbf{a}_i \cos\boldsymbol{\theta}_i \tag{20}$$

Step 4 If $\|\mathbf{r}_k\|_2 < \varepsilon$, stop, where ε is a chosen residual threshold. Otherwise, set $k = k+1$ and go to Step 2.

The performance of this algorithm depends on the assumption that the components of the underlying decomposition are approximately orthogonal to each other.

3. IDENTIFICATION OF TIME-VARYING TENSION IN BRIDGE CABLES

According to the widely used flat taut string theory that neglects both sag-extensibility and bending stiffness, a constant cable tension force F can be calculated by

$$F = 4mL^2\left(\frac{\omega_n}{2\pi n}\right)^2 \tag{21}$$

where ω_n denotes the nth natural frequency in radian/s; and m and L are the mass density and length of the cable, respectively. Given the measured frequency for the nth mode number, the cable tension can be calculated directly from Eqn (21).

Consider a slowly time-varying cable tension force $F(t_j), j = 1, \ldots, N$, then Eqn (21) is expressed as

$$F(t_j) = 4mL^2\left(\frac{\omega_n(t_j)}{2\pi n}\right)^2 \tag{22}$$

where $\omega_n(t_j)$ is the time-varying nth natural frequency.

An important and useful feature of the flat taut string theory for vibration of a cable is that the natural frequencies of the higher modes are integer multiples of the fundamental frequency, that is $\omega_n(t) = n\omega_1(t)$. This feature means that we only need to calculate one instantaneous frequency, which significantly simplifies the algorithm.

3.1. Improved algorithm for identification of time-varying frequencies of cable vibration signals

Here, the continuous signal, $f(t)$, is the acceleration at time t, and the vector $\mathbf{f}$ is the samples of $f(t)$ at discrete time $t_j, j = 1, \ldots, N$. If the number of samples, N, is large enough such that $f(t)$ can be well approximated by $\mathbf{f}$, the algorithm in Section 2 works. Moreover, if we only need one instantaneous frequency, then iteration is not necessary. We only need to solve one nonlinear least-squares problem

$$\min_{(a_k)_{1\le k\le K},\ \theta_1} \left\| f(t) - \sum_{k=1}^{K} a_k(t)\cos k\theta_1(t) \right\|_2^2, \text{ subject to : } a_k(t) \in V(\theta_1),\ \dot{\theta}_1(t) \in V(\theta_1) \tag{23}$$

Here, K is the number of modes used to calculate the instantaneous frequency which is a given positive integer. The corresponding discrete version is

$$\min_{\mathrm{x},\ \theta_1} \left\| \mathbf{f} - \widetilde{\boldsymbol{\Phi}}_{\theta_1} \cdot \mathbf{x} \right\|_2^2, \text{ subject to : } \dot{\boldsymbol{\theta}}_1 \in V(\boldsymbol{\theta}_1) \tag{24}$$

where $\widetilde{\boldsymbol{\Phi}}_\theta$ is a $N \times K(2\lambda L_\theta + 1)$ dimensional matrix

$$\widetilde{\boldsymbol{\Phi}}_{\theta_1} = \left[\boldsymbol{\Phi}_{\theta_1}, \ldots, \boldsymbol{\Phi}_{(K\theta_1)}\right] \tag{25}$$

and each $\boldsymbol{\Phi}_{(k\theta)}$, $k = 1, \ldots, K$ is a $N \times (2\lambda L_\theta + 1)$ matrix whose jth row is defined as follows:

$$\boldsymbol{\Phi}_{(k\boldsymbol{\theta}_1),j} = \left(\cos k\boldsymbol{\theta}_1(t_j)\right)\boldsymbol{\Pi}_{\theta_1,j},\ j = 1, \ldots, N \tag{26}$$

and $\boldsymbol{\Pi}_{\theta_1,j}$ is defined in Eqn (17).

The above nonlinear least-squares problem is solved by a Gauss–Newton type iteration method which is described below as the adaptive sparse time frequency analysis (AS-TFA) Algorithm. The explanation of this algorithm can be found in reference [23]. The difference is that only $\boldsymbol{\theta}_1$ needs to be optimized.

DOI: 10.1002/stc

To start the AS-TFA Algorithm, we need an initial guess of the phase function. Gauss–Newton type iteration is known to be sensitive to the initial guess. In general, it is not an easy task to find a good initial guess. In order to abate the dependence on the initial guess, we replace λ in Eqn (7) by η in the step of updating $\boldsymbol{\theta}_1$. When η is small, $\dot{\boldsymbol{\theta}}_1$ is confined to a smaller space, so that the objective functional is expected to have fewer extrema. The iterations may then find a good approximation for $\dot{\boldsymbol{\theta}}_1$ in this smaller space. Then we gradually increase η up to λ, so correspondingly, the space for $\dot{\boldsymbol{\theta}}_1$ is enlarged, which allows for more detail in $\dot{\boldsymbol{\theta}}_1$. The parameter $\Delta\eta$ in step 7 of the algorithm, which is used to increase η, is chosen to be $\lambda/10$.

AS-TFA Algorithm

Input: Initial guess of phase function $\boldsymbol{\theta}_1^0 = \boldsymbol{\theta}_0$ and parameters $\eta = 0$, λ, ε_0.
Output: Phase function $\boldsymbol{\theta}_1$

1. **while** $\eta < \lambda$ do
2. **while** $\left\|\boldsymbol{\theta}_1^{n+1} - \boldsymbol{\theta}_1^n\right\|_2 > \varepsilon_0$ do
3. Solve the following least-squares problem:

$$\left(\mathbf{a}_k^{n+1}, \mathbf{b}_k^{n+1}\right) = \underset{\mathbf{x},\mathbf{y}}{\operatorname{argmin}} \left\|\mathbf{f} - \left(\widetilde{\boldsymbol{\Phi}}_{\theta_1^n}\cdot\mathbf{x} + \widetilde{\boldsymbol{\Psi}}_{\theta_1^n}\cdot\mathbf{y}\right)\right\|_2^2$$

where $\widetilde{\boldsymbol{\Phi}}_{\theta_1^n}$ is defined in Eqn (25) by replacing $\boldsymbol{\theta}_1$ with $\boldsymbol{\theta}_1^n$, $\widetilde{\boldsymbol{\Psi}}_{\theta_1^n}$ is also a $N\times(2\lambda L_\theta+1)$ dimensional matrix which has the same structure as $\widetilde{\boldsymbol{\Phi}}_{\theta_1^n}$.

$$\widetilde{\boldsymbol{\Psi}}_{\theta_1^n} = \left[\boldsymbol{\Psi}_{\theta_1^n}, \ldots, \boldsymbol{\Psi}_{\left(K\theta_1^n\right)}\right]$$

and the jth row of $\boldsymbol{\Psi}_{\left(k\theta_1^n\right),j}$, $k = 1, \ldots, K$ is

$$\boldsymbol{\Psi}_{\left(k\theta_1^n\right),j} = \sin\left(k\theta_1^n\left(t_j\right)\right)\boldsymbol{\Pi}_{\theta^n,j}$$

$\boldsymbol{\Pi}_{\theta^n,j}$ is given in Eqn (17).

4. Calculate the envelopes $\mathbf{a}_k$, $\mathbf{b}_k$, $k = 1, \ldots, K$:

$$\mathbf{a}_k = \boldsymbol{\Pi}_{\theta^n}\cdot\widetilde{\mathbf{a}}_k^{n+1},\ \mathbf{b}_k = \boldsymbol{\Pi}_{\theta^n}\cdot\widetilde{\mathbf{b}}_k^{n+1}$$

where $\widetilde{\mathbf{a}}_k^{n+1}$, $\widetilde{\mathbf{b}}_k^{n+1}$, $k = 1, \ldots, K$ are all $2\lambda L_\theta + 1$ dimensional vectors

$$\widetilde{\mathbf{a}}^{n+1} = \left[\widetilde{\mathbf{a}}_1^{n+1}, \ldots, \widetilde{\mathbf{a}}_K^{n+1}\right],\ \widetilde{\mathbf{b}}^{n+1} = \left[\widetilde{\mathbf{b}}_1^{n+1}, \ldots, \widetilde{\mathbf{b}}_K^{n+1}\right]$$

which are divided corresponding to the construction of $\widetilde{\boldsymbol{\Phi}}_{\theta^n}$ and $\widetilde{\boldsymbol{\Psi}}_{\theta_1^n}$.

5. Update $\boldsymbol{\theta}_1^n$:

$$\Delta\theta_k\left(t_j\right) = \sum_{l=1}^{j}\Delta\,\dot{\theta}_k(t_l),\ j = 1, \ldots, N,\ \Delta\,\dot{\theta}_k\left(t_j\right) = P_{V\left(\theta_1^n;\eta\right)}\left(\nabla_0\left(\arctan\left(\frac{b_k\left(t_j\right)}{a_k\left(t_j\right)}\right)\right)\right)$$

and

$$\theta_1^{n+1}\left(t_j\right) = \theta_1^n\left(t_j\right) - \sum_{k=1}^{K}\omega_k\left(t_j\right)\Delta\theta_k\left(t_j\right),\ \ \omega_k\left(t_j\right) = \left(a_k^2\left(t_j\right) + b_k^2\left(t_j\right)\right)\left(\sum_{k=1}^{K}\left(a_k^2\left(t_j\right) + b_k^2\left(t_j\right)\right)\right)^{-1}$$

where $P_{V\left(\theta_1^n;\eta\right)}$ is the projection operator to the space $V\left(\boldsymbol{\theta}_1^n;\eta\right)$; $V\left(\boldsymbol{\theta}_1^n;\eta\right)$ is the space defined in Eqn (7) with $\lambda = \eta$ and ∇_0 is the central difference operator.

6. **end while**
7. $\eta = \eta + \Delta\eta$
8. **end while**

DOI: 10.1002/stc

After we obtain the solution $\widetilde{\theta}_1(t_j), j=1,\ldots,N$, the fundamental modal frequency is $\widetilde{\omega}_1(t_j) = \dot{\widetilde{\theta}}_1(t_j)$, where $\dot{\widetilde{\theta}}_1(t_j)$ is calculated by central difference on $\widetilde{\theta}_1(t_j)$. Then, the time-varying cable tension force $\widetilde{F}(t_j)$ is estimated as

$$\widetilde{F}(t_j) = 4mL^2\left(\frac{\widetilde{\omega}_1(t_j)}{2\pi}\right)^2 \tag{27}$$

4. CABLE EXPERIMENTS

4.1. Experimental set-up

An experiment with a model cable of 1403 cm length (Figure 2) was carried out by Li *et al.* [17], and it is employed here to illustrate the proposed approach. The similar cable experiment model also has been used by other researchers [29–31]. The vibration of the cable is excited by two 550 kW blower fans to simulate wind. A force sensor that is installed between the left anchorage of the cable and the sliding bearing is used to measure the time-varying cable tensions. A threaded rod is installed in a series connection with the cable to adjust the cable tension in real time, as shown in Figure 2(b); the threaded rod is operated manually to generate the cable tension variation. Two accelerometers are placed at 2.43 and 3.60 m from the sliding bearing to measure the in-plane and out-of-plane vibrations of the cable. The dSPACE CP1103 (GmbH, Paderborn, Germany) data acquisition system is used to record the acceleration and cable tension force data with a sampling frequency of 200 Hz.

Three experimental cases are considered:

Case 1 the initial cable tension is 6500 N, the variation of cable force is 15% with duration of 25 s;
Case 2 the initial cable tension is 6500 N, the variation of cable force is 20% with duration of 25 s;
Case 3 the initial cable tension is 6500 N, the variation of cable force is from 5%, 10%, 15% and 20% with duration of 30, 25, 30 and 30 s, respectively.

4.2. Identification results

4.2.1. Identification results for Case 1. For Case 1, the measured cable acceleration signal and its Fourier amplitude spectrum within a frequency range of [2,15] Hz are shown in Figure 3.

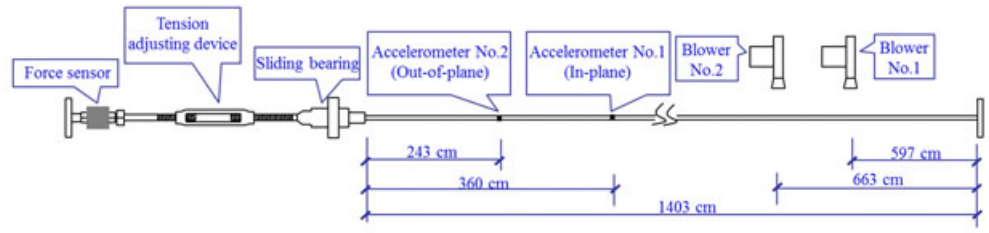

(a)

(b) (c) (d)

Figure 2. Experimental setup: (a) experimental model; (b) tension adjusting device; (c) data acquisition system and (d) blowers and cable.

DOI: 10.1002/stc

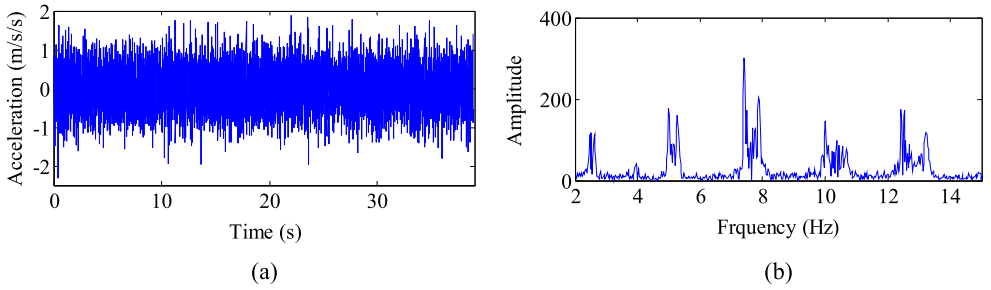

Figure 3. Measured acceleration and the Fourier transform of the signal for Case 1: (a) acceleration data; and (b) Fourier amplitude spectrum.

Figure 3(b) clearly shows the first five modal frequencies of the cable are very close to being integer multiples of 1, 2, 3, 4 and 5 of the fundamental frequency around 2.57 Hz.

For applying the AS-TFA Algorithm to the measured acceleration data to identify each time-varying modal frequency, the first five modal responses in the time domain are separated from the signal shown in Figure 3 by narrow-band filtering and the time axis is normalized to [0, 1] as shown in Figure 4. The corresponding frequency intervals of the signal in Figure 4 are [2.32, 2.83] Hz, [4.64, 5.66] Hz, [6.90, 8.49] Hz, [9.28, 11.32] Hz and [11.60, 14.15] Hz, respectively, which are centred on the estimates of the modal frequencies: $f_1 = 2.57$ Hz, $f_2 = 5.15$ Hz, $f_3 = 7.72$ Hz, $f_4 = 10.29$ Hz and $f_5 = 12.87$ Hz.

The selection of the initial phase is important when using the AS-TFA algorithm. For some signals where the frequency significantly changes with time, it is difficult to obtain the initial phase. Fortunately, for the vibration signals of bridge cables, the time variation of the frequency caused by vehicles and wind is usually relatively small. Therefore, the initial phase can be readily

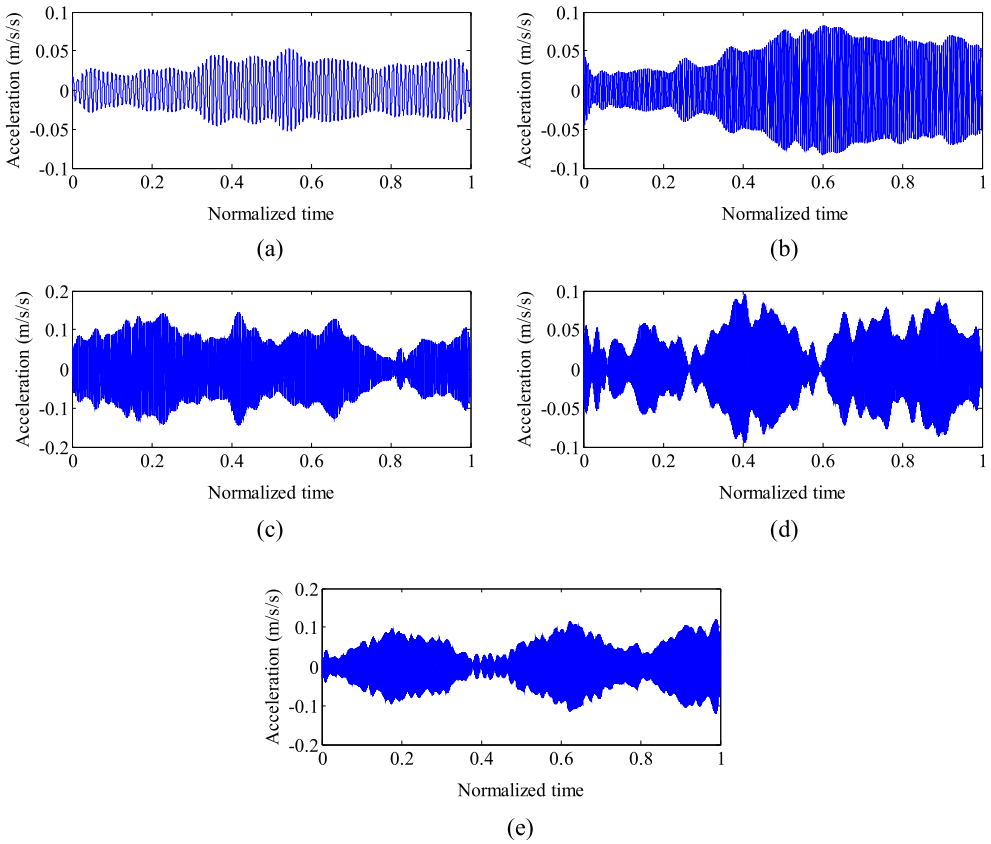

Figure 4. The separated first five mode responses in the time domain.

DOI: 10.1002/stc

estimated from the modal frequencies which are obtained by picking a modal peak in the frequency domain

$$\boldsymbol{\theta}_0 = 2\pi \frac{nf_k}{f}\mathbf{v} \tag{28}$$

where n is the length of signal; f_k is the k^{th} modal frequency; f is the sampling frequency ($f=200$ Hz in this example); and $\mathbf{v}=[0:1/(n-1):1]^T$ is a normalized time axis vector. The initial phase for the AS-TFA algorithm can be calculated using Eqn (28) for each of the first five modal frequencies with sample length $n=7774$ giving $\boldsymbol{\theta}_0=628.40\mathbf{v}$, $1256.80\mathbf{v}$, $1885.2\mathbf{v}$, $2513.60\mathbf{v}$ and $3142.00\mathbf{v}$, respectively.

Applying the AS-TFA algorithm to each modal response in Figure 4, the identified time-frequency results of Case 1 are shown in Figure 5(a) for the first five time-varying modal frequencies. For comparison, the Hilbert–Huang transform (HHT) calculated using the Matlab Toobox developed by N. Huang *et al.* (http://rcada.ncu.edu.tw/research1.htm) is also employed to identify the first five time-varying modal frequencies, and the results are shown in Figure 5(b). Figure 5 shows that the identified time-varying modal frequencies by AS-TFA algorithm are much smoother and more stable than the HHT results.

Using each of these five time-varying frequencies to calculate the cable tension forces by Eqn (27), the results are shown in Figure 6, where the solid lines (labelled 'Measured') are the cable tension forces measured by the force sensor without de-noising in the experiments, the dotted lines (labelled 'HHT') are the identified cable tension forces by the HHT method, and the dashed lines (labelled 'AS-TFA') are the identified cable tension forces by the AS-TFA method. As shown in Figure 6, the identified time-varying cable tension forces are close to the measured cable tension forces, especially for the AS-TFA Algorithm. The calculated cable tension forces from the HHT method in Figure 6 are much more noisy, especially for the fourth and fifth time-varying modal frequencies. To quantify the identification error, the relative error of the cable tension force is calculated by

$$\xi_a = \frac{\left\|\widetilde{\mathbf{F}}_a - \mathbf{T}\right\|_2}{\|\mathbf{T}\|_2} \times 100\% \tag{29}$$

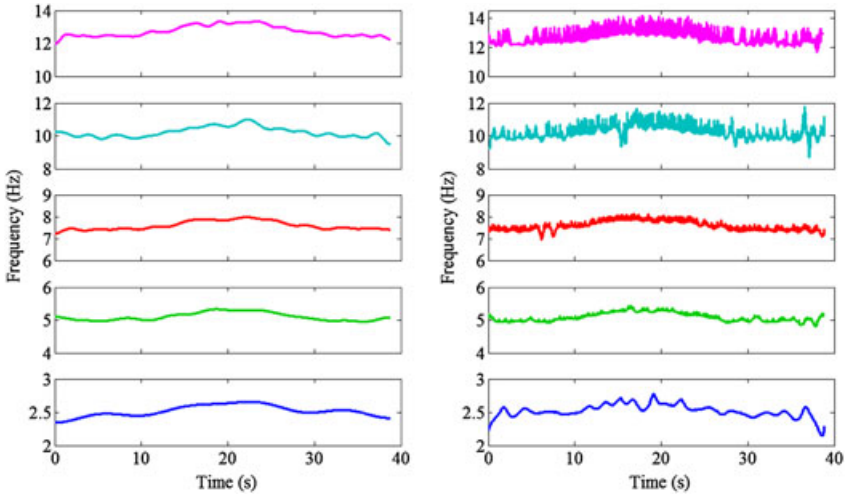

(a) (b)

Figure 5. Identified first five time-varying frequencies for Case 1: (a) adaptive sparse time frequency analysis; and (b) Hilbert–Huang transform.

DOI: 10.1002/stc

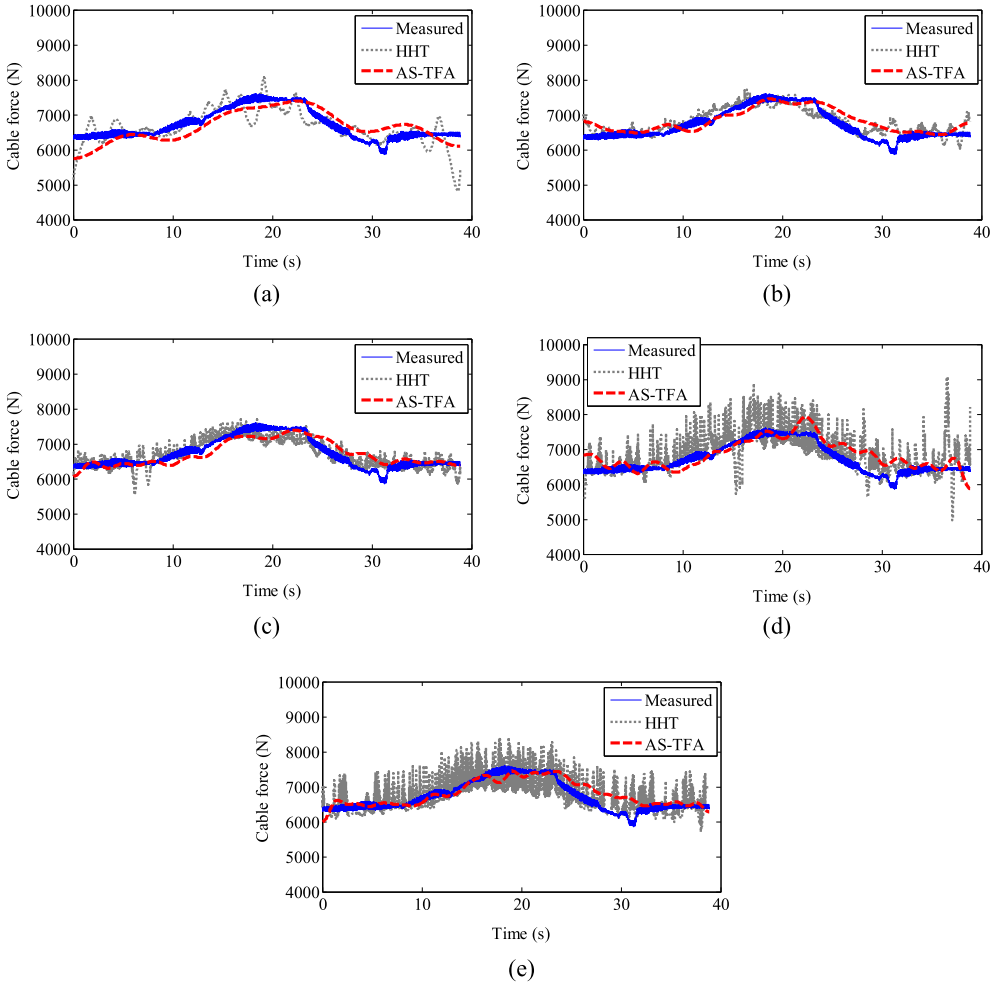

Figure 6. Identified time-varying cable tension forces of Case 1 using the first five time-varying modal frequencies from adaptive sparse time frequency analysis (AS-TFA) and Hilbert–Huang transform (HHT), which are shown from (a) to (e) from the first through to the fifth modal frequency.

$$\xi_h = \frac{\left\|\widetilde{\mathbf{F}}_h - \mathbf{T}\right\|_2}{\|\mathbf{T}\|_2} \times 100\% \tag{30}$$

where ξ_a and ξ_h are the percentage identification errors of the cable-tension forces identified by adaptive sparse time-frequency and HHT based methods, respectively; $\widetilde{\mathbf{F}}_a = \left[\widetilde{F}_a(t_1), \ldots, \widetilde{F}_a(t_N)\right]$ and $\widetilde{\mathbf{F}}_h = \left[\widetilde{F}_h(t_1), \ldots, \widetilde{F}_h(t_N)\right]$ are the identified cable tension force vectors for these two methods; and $\mathbf{T} = [T(t_1), \ldots, T(t_N)]$ is the measured cable tension force at the sampled times. The identification errors for the cable tension forces calculated using the identified first to fifth time-varying modal frequencies from the AS-TFA algorithm are: $\xi_a = 4.26\,\%$, 3.62%, 3.27%, 4.36% and 3.43%, respectively. The identification errors for the cable tension forces calculated using the identified first to fifth time-varying modal frequencies by using the HHT method are: $\xi_h = 5.29\,\%$, 3.34%, 3.41%, 5.83% and 5.20%, respectively.

Figure 6 shows that the time-varying cable forces estimated using each identified modal frequency have some differences. We now impose the constraints between the higher-order modal frequencies and the fundamental frequency of the cable and set the parameter $K = 5$ and the initial phase

DOI: 10.1002/stc

$\boldsymbol{\theta}_0 = 628.40\mathbf{v}$ in the AS-TFA Algorithm. The identification results obtained from AS-TFA Algorithm are shown in Figure 7, where the identified time-varying cable force for Case 1 is smooth and stable, and it has a corresponding identification error of $\xi_a = 3.34\,\%$.

4.2.2. Identification results for Case 2. For Case 2, the measured cable acceleration signal with length $n = 8630$ and its Fourier amplitude spectrum within a frequency range of [2,15] Hz are shown in Figure 8.

With the same calculation procedure as used in Case 1, applying the AS-TFA Algorithm to the first five modal responses separated from the measured acceleration data, which are shown in Figure 8(a), leads to the identified time-frequency results of Case 2 that are shown in Figure 9(a), which clearly shows the first five time-varying modal frequencies. Comparing with the identification results by using the HHT method, which are shown in Figure 9(b), the adaptive sparse time frequency analysis method obviously produces much better results.

The time-varying cable tension force identification results of Case 2 are shown in Figure 10, which shows that the time-varying cable tension force can be well identified by the adaptive sparse time-frequency analysis method with small identification error compared with the HHT based results. The corresponding cable tension force identification error for both of these methods are: $\xi_a = 3.76\,\%$, 3.62%, 3.53%, 4.25%, 3.46%; and: $\xi_h = 8.84\,\%$, 8.30%, 5.69%, 5.94%, 7.15%, respectively. The identification results from combining the first five time-varying modal frequencies are also smoother and more stable than the results identified from each signal frequency, as shown in Figure 11, where the identification error is 3.58%.

4.2.3. Identification results for Case 3. For the more complex scenario of Case 3, the measured cable acceleration signal length $n = 56\,999$ and its Fourier amplitude spectrum within a frequency range of [2,15] Hz are shown in Figure 12.

The identified time-frequency results for Case 3 from using the adaptive sparse time-frequency and HHT methods are shown in Figure 13. Obviously, the adaptive sparse time-frequency based results are

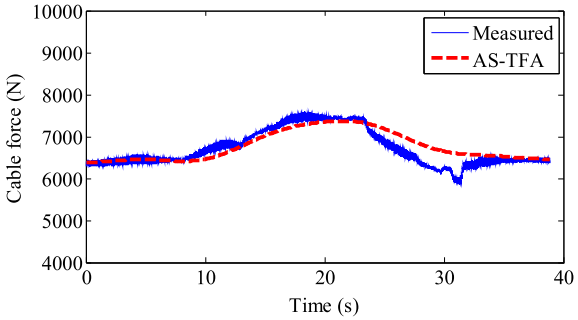

Figure 7. Identified time-varying cable tension force for Case 1 by combining the first five time-varying frequencies, with the identification error $\xi_a = 3.34\,\%$. AS-TFA, adaptive sparse time frequency analysis.

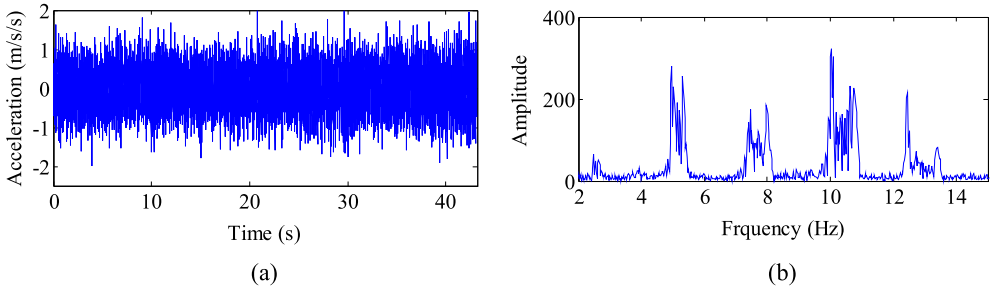

Figure 8. Measured acceleration and the Fourier transform of the signal for Case 2: (a) acceleration data; and (b) Fourier amplitude spectrum.

DOI: 10.1002/stc

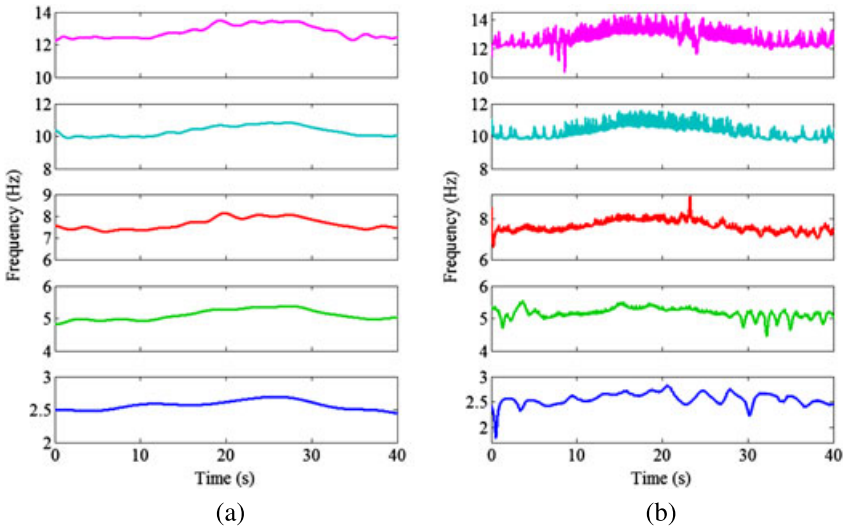

Figure 9. Identified first five time-varying frequencies for Case 2: (a) adaptive sparse time frequency analysis; and (b) Hilbert–Huang transform.

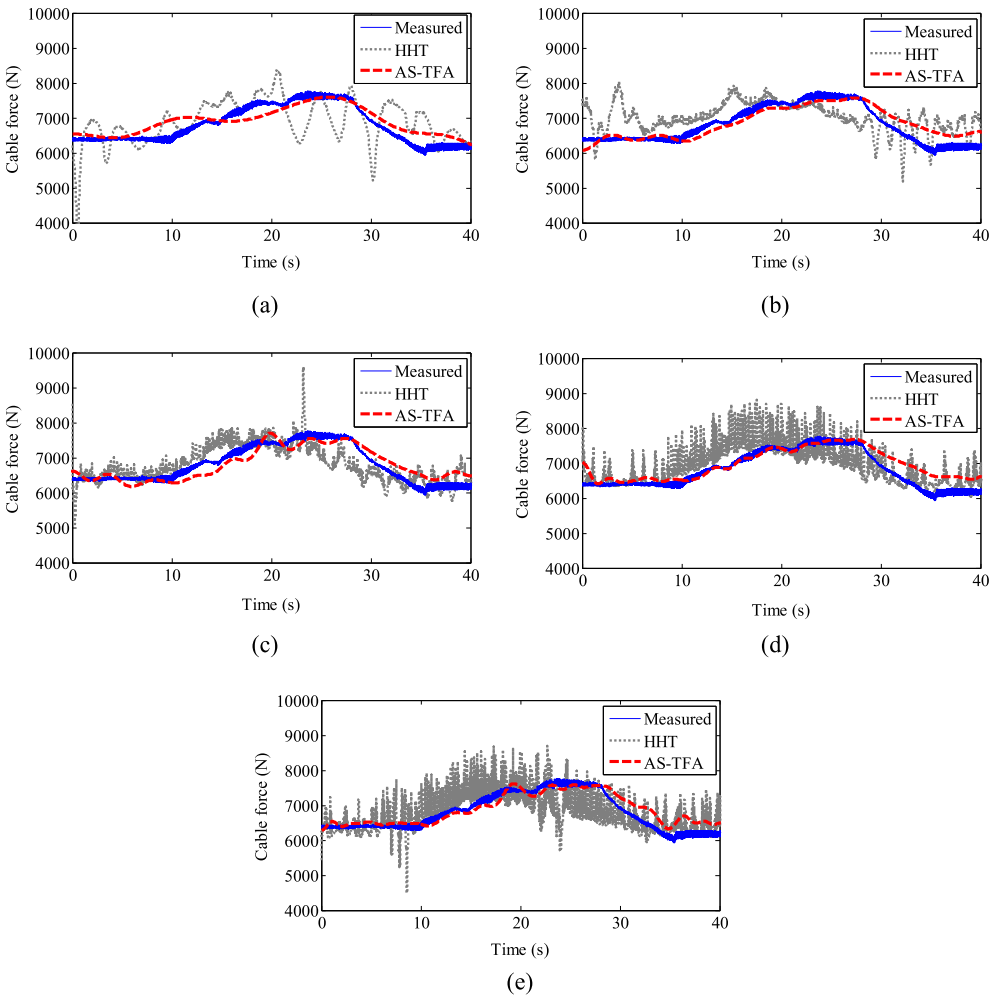

Figure 10. Identified time-varying cable tension forces of Case 2 using the first five time-varying frequencies from adaptive sparse time frequency analysis (AS-TFA) and Hilbert–Huang transform (HHT), which are shown from (a) to (e) for the first through to the fifth modal frequency.

DOI: 10.1002/stc

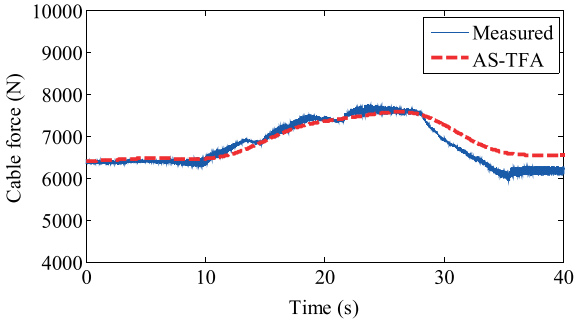

Figure 11. Identified time-varying cable tension force of Case 2 by combining the first five time-varying frequencies, with the identification error $\xi_a = 3.58\,\%$. AS-TFA, adaptive sparse time frequency analysis.

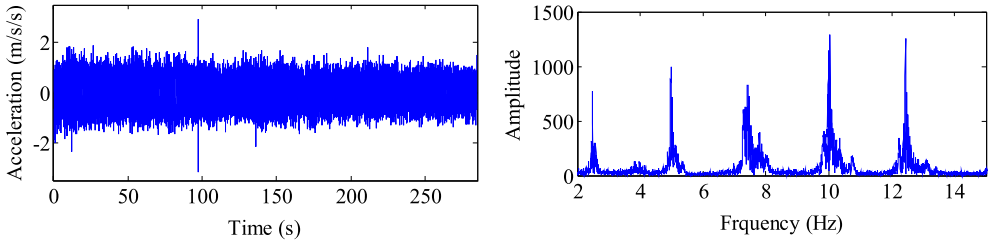

Figure 12. Measured acceleration and the Fourier transform of the signal for Case 3: (a) acceleration data; and (b) Fourier amplitude spectrum.

much smoother and more stable than the HHT based results. Using each of these five time-varying frequencies, the calculated time-varying cable tension forces are shown in Figure 14, which shows that the AS-TFA based identification results are close to the measured cable forces, with relative identification errors: $\xi_a = 3.04\,\%$, 2.96%, 2.56%, 2.50% and 2.26% for each of the five time-varying modal frequencies. However, the corresponding identification errors for the HHT based results are significantly larger: $\xi_h = 5.62\,\%$, 4.23%, 5.19%, 5.36% and 5.98%, respectively. In this case, the results obtained by

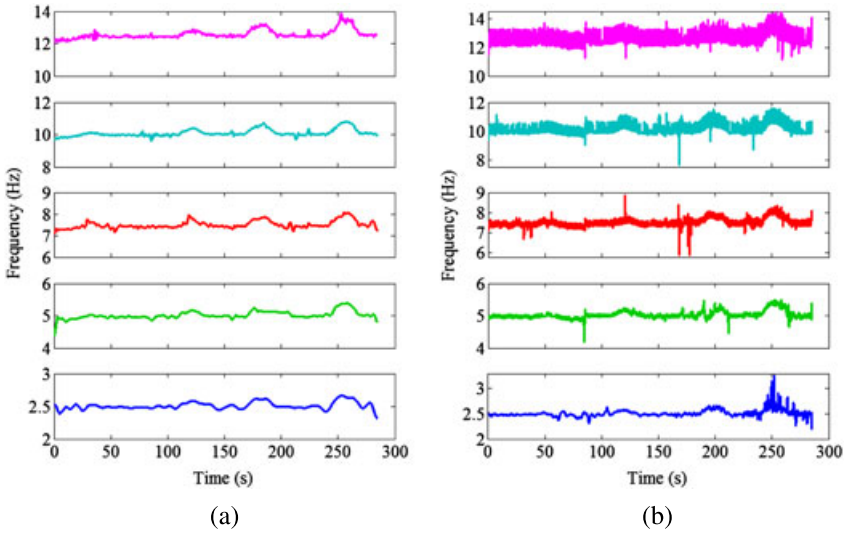

Figure 13. Identified first five time-varying frequencies for Case 3: (a) adaptive sparse time frequency analysis; and (b) Hilbert–Huang transform.

DOI: 10.1002/stc

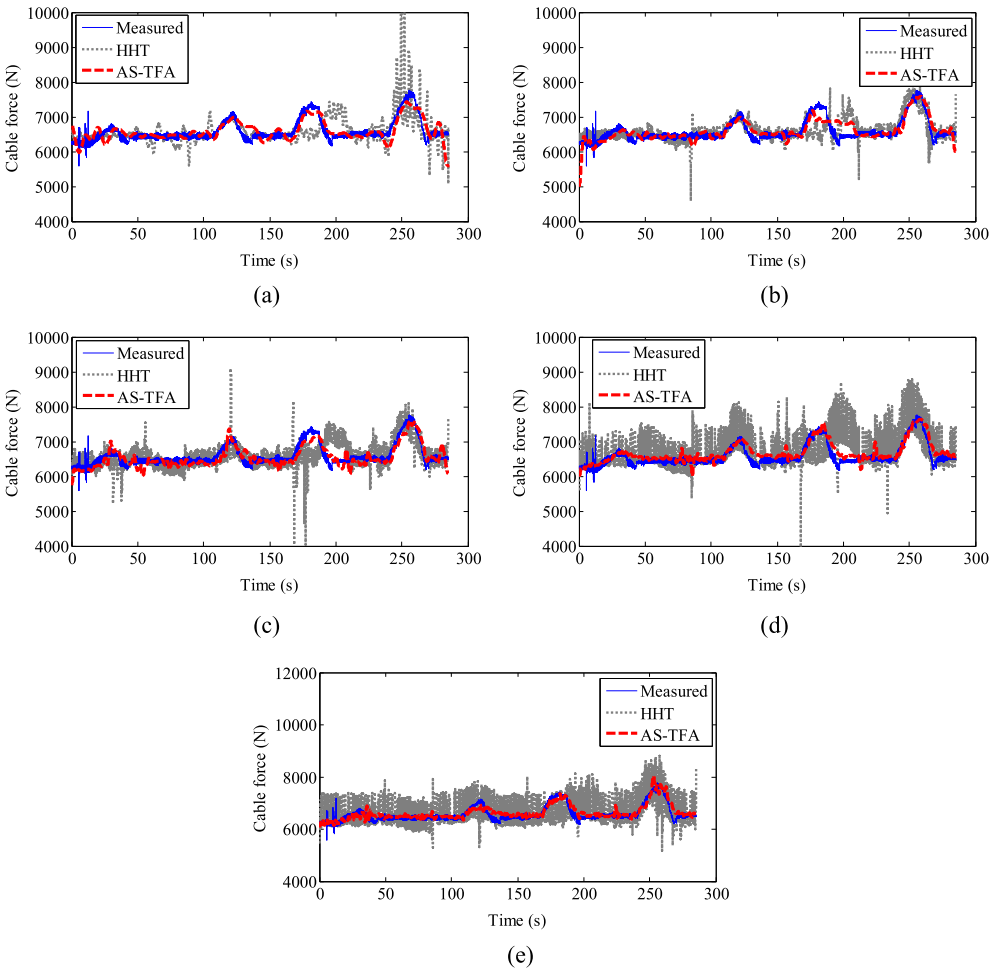

Figure 14. Identified time-varying cable tension forces of Case 3 using the first five time-varying modal frequencies from adaptive sparse time frequency analysis (AS-TFA) and (HHT), which are shown from (a) to (e) for the first through to the fifth modal frequency.

HHT are much more noisy, and the real variations of the cable tension forces are not well identified. The identification result in Figure 15 shows the improvement from combining the first five time-varying modal frequencies in the AS-TFA Algorithm with $K=5$ and the initial phase calculated by Eqn (28), with the identification error being $\xi_a = 1.95\,\%$.

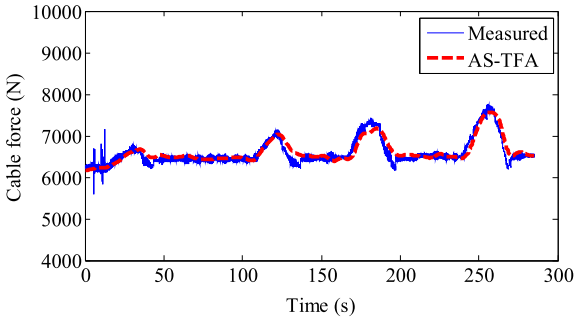

Figure 15. Identified time-varying cable tension force of Case 3 by combining the first five time-varying frequencies; with the identification error $\xi_a = 1.95\,\%$. AS-TFA, adaptive sparse time frequency analysis.

DOI: 10.1002/stc

5. CONCLUSIONS

A time-varying cable tension force identification method based on adaptive sparse time-frequency analysis is proposed in this paper where the first step is to estimate the time-varying modal frequencies from a cable vibration signal, and the second step is to use these results to calculate the time-varying cable tension force by flat taut string theory. Additional robustness of the method is provided by considering the integer ratios of the different modal frequencies to the fundamental frequency of the cable in the adaptive sparse time-frequency algorithm.

The results of cable experiments show that the time-varying modal frequencies of the cable can be well identified by the proposed adaptive sparse time-frequency algorithm and that the time-varying cable tension forces calculated from each time-varying frequency separately are close to the force sensor measurements. A comparison of the results obtained from the HHT method and the proposed approach show that the latter results are much more stable and have smaller identification errors. The identified first five time-varying modal frequencies from the cable experiment can be combined to produce more accurate and more robust results. The relative identification errors of the time-varying cable tension forces for all three experimental scenarios are less than 5%, which is an acceptable error for structural health monitoring purposes.

We expect that the procedure of looking for the sparsest decomposition among all feasible decompositions based on a redundant time-frequency dictionary could also be achieved using a Bayesian model selection method. For future research, it would be interesting to develop a Bayesian method for sparse time-frequency analysis for the identification of time-varying cable tension forces and compare the results with the approach proposed in this paper.

ACKNOWLEDGEMENTS

One of the authors (Yuequan Bao) acknowledges the support provided by the China Scholarship Council while he was a Visiting Associate at the California Institute of Technology. This research was also supported by grants from the National Basic Research Program of China (Grant No.2013CB036305), the National Natural Science Foundation of China (Grant No. 51378154, 51161120359), which supported the first and fourth authors (Yuequan Bao and Hui Li). The research of Zuoqiang Shi was supported by National Natural Science Foundation of China (Grant No. 11371220). The research of Thomas Hou and Zuoqiang Shi was also in part supported by National Science Foundation of USA (Grant DMS-1318377).

REFERENCES

1. Ou J, Li H. Structural health monitoring in mainland China: review and future trends. *Structural Health Monitoring* 2010; **9**(3):219–232.
2. Mufti AA. Structural health monitoring of innovative Canadian civil engineering structures. *Structural Health Monitoring* 2002; **1**(1):89–103.
3. Ko JM, Ni YQ. Technology developments in structural health monitoring of large-scale bridges. *Engineering Structures* 2005; **27**(12):1715–1725.
4. Jang S, Jo H, Cho S, Mechitov K, Rice JA, Sim SH, Jung HJ, Yun CB, Spencer BF Jr, Agha G. Structural health monitoring of a cable-stayed bridge using smart sensor technology: deployment and evaluation. *Smart Structures and Systems* 2010; **6**(5-6):439–459.
5. Kim BH, Park T. Estimation of cable tension force using the frequency-based system identification method. *Journal of Sound and Vibration* 2007; **304**:660–676.
6. Casas JR. A combined method for measuring cable forces: the cable-stayed Alamillo Bridge, Spain. *Structural Engineering International* 1994; **4**(4):235–240.
7. Gentile C. Deflection measurement on vibrating stay cables by non-contact microwave interferometer. *NDT & E International* 2010; **43**(3):231–240.
8. Kim BH, Shin HY. A comparative study of the tension estimation methods for cable supported bridges. *International Journal of Steel Structures* 2007; **7**(1):77–84.
9. Ren WX, Liu HL, Chen G. Determination of cable tensions based on frequency differences. *Engineering Computations* 2008; **25**(2):172–189.
10. Russell JC, Lardner TJ. Experimental determination of frequencies and tension for elastic cables. *Journal of Engineering Mechanics* 1998; **124**(10):1067–1072.
11. Humar JL. *Dynamics of Structures*. Prentice Hall: Upper Saddle River, NJ, 2000.
12. Fang Z, Wang J. Practical formula for cable tension estimation by vibration method. *Journal of Bridge Engineering* 2012; **17**:161–164.
13. Sim SH, Li J, Jo H, Park JW, Cho S, Spencer BF Jr, Jung HJ. A wireless smart sensor network for automated monitoring of cable tension. *Smart Materials and Structures* 2014; **23**(2):025006.

DOI: 10.1002/stc

14. Zui H, Shinke T, Namita YH. Practical formulas for estimation of cable tension by vibration method. *ASCE Journal of Structural Engineering* 1996; **122**(6):651–656.
15. Liao W, Ni Y, Zheng G. Tension force and structural parameter identification of bridge cables. *Advances in Structural Engineering* 2012; **15**(6):983–996.
16. Cho S, Lynch JP, Lee JJ, Yun CB. Development of an automated wireless tension force estimation system for cable-stayed bridges. *Journal of Intelligent Material Systems and Structures* 2010; **21**(3):361–376.
17. Li H, Zhang F, Jin Y. Real-time identification of time-varying tension in stay cables by monitoring cable transversal acceleration. *Structural Control Health Monitoring* 2014; **21**:1100–1111.
18. Yang Y, Li S, Nagarajaiah S, Li H, Zhou P. Real-time output-only identification of time-varying cable tension from accelerations via Complexity Pursuit. *ASCE Journal of Structural Engineering* 2015; **142**(1): 04015083.
19. Wang LM, Wang G, Zhao Y. Application of EM stress sensors in large steel cables. In *Sensing Issues in Civil Structural Health Monitoring*, Ansari F (ed). Springer: Berlin, Germany, 2005; 145–154.
20. Sumitro S, Kurokawa S, Shimano K, Wang ML. Monitoring based maintenance utilizing actual stress sensory technology. *Smart Materials and Structures* 2005; **14**:S68–S78.
21. Yim J, Wang ML, Shin SW, Yun CB, Jung HJ, Kim JT, Eem SH. Field application of elasto-magnetic stress sensors for monitoring of cable tension force in cable-stayed bridges. *Smart Structural and Systems* 2013; **12**(3-4):465–482.
22. Hou TY, Shi Z. Adaptive data analysis via sparse time-frequency representation. *Advances in Adaptive Data Analysis* 2011; **3**(1&2):1–28.
23. Hou TY, Shi Z. Data-driven time-frequency analysis. *Applied and Computational Harmonic Analysis* 2013; **35**(2):284–308.
24. Hou TY, Shi Z, Tavallali P. Convergence of a data-driven time-frequency analysis method. *Applied and Computational Harmonic Analysis* 2014; **37**(2):235–270.
25. Huang NE, Shen Z, Long SR, Wu MC, Shih HH, Zheng Q, Yen NC, Tung CC, Liu HH. The empirical mode decomposition and the Hilbert spectrum for nonlinear and non-stationary time series analysis. *Proceedings of the Royal Society of London A: Mathematical, Physical and Engineering Sciences* 1998; **454**:903–995.
26. Candes EJ. Compressive sampling. *Proceedings of the International Congress of Mathematicians*, Madrid, Spain, 2006: 1433–1452.
27. Donoho D. Compressed sensing. *IEEE Transactions on Information Theory* 2006; **52**(4):1289–1306.
28. Baraniuk R. Compressive sensing. *IEEE Signal Processing Magazine* 2007; **24**(4):118–121.
29. Casciati F, Ubertini F. Nonlinear vibration of shallow cables with semiactive tuned mass damper. *Nonlinear Dynamics* 2008; **53**(1-2):89–106.
30. Faravelli L, Ubertini F. Nonlinear state observation for cable dynamics. *Journal of Vibration and Control* 2009; **15**(7):1049–1077.
31. Faravelli L, Fuggini C, Ubertini F. Toward a hybrid control solution for cable dynamics: theoretical prediction and experimental validation. *Structural Control and Health Monitoring* 2010; **17**(4):386–403.

DOI: 10.1002/stc